Detection of iodine monoxide radicals in the marine boundary layer using laser induced fluorescence spectroscopy

Whalley, LK; Furneaux, KL; Gravestock, T; Atkinson, HM; Bale, CSE; Ingham, T; Bloss, William; Heard, DE

DOI:
10.1007/s10874-007-9075-9

Document Version
Publisher's PDF, also known as Version of record

Citation for published version (Harvard):
Whalley, LK, Furneaux, KL, Gravestock, T, Atkinson, HM, Bale, CSE, Ingham, T, Bloss, W & Heard, DE 2007, 'Detection of iodine monoxide radicals in the marine boundary layer using laser induced fluorescence spectroscopy', *Journal of Atmospheric Chemistry*, vol. 58, pp. 19-39. https://doi.org/10.1007/s10874-007-9075-9

J Atmos Chem (2007) 58:19–39
DOI 10.1007/s10874-007-9075-9

Detection of iodine monoxide radicals in the marine boundary layer using laser induced fluorescence spectroscopy

Lisa K. Whalley · Kate L. Furneaux · Tom Gravestock · Helen M. Atkinson · Catherine S. E. Bale · Trevor Ingham · William J. Bloss · Dwayne E. Heard

Received: 22 March 2007 / Accepted: 25 May 2007 /
Published online: 8 August 2007

Abstract A Laser Induced Fluorescence (LIF) instrument has been developed to detect iodine monoxide (IO) radicals in the atmosphere. An all solid-state Nd:YAG pumped Ti:Sapphire laser operating at approximately 445 nm was used to excite the (2,0) band of the IO $A^2\Pi_{3/2} \leftarrow X^2\Pi_{3/2}$ electronic transition, with off-resonance fluorescence in the (2,5) band detected at 521 nm. The sensitivity of the instrument was determined by calibration. IO (between 10 and 150 pptV) was generated following the 184.9 nm photolysis of $N_2O/CF_3I/N_2$ mixtures with O_3 actinometry used to determine the photolysis flux. The detection limit was determined to be 0.3 pptV for a 300 s integration period, with an uncertainty of 23% (1σ). The instrument was deployed in August/September 2006 during the RHaMBLe (Reactive Halogens in the Marine Boundary Layer) campaign in Roscoff, France. Located on a small jetty, a few metres from the water's edge at high tide, the instrument measured significant levels of IO on 11 days, with a maximum of 27.6±3.2 pptV observed on one day (averaged over 10 s) representing the highest IO mixing ratio recorded in the marine boundary layer to date. IO displayed a clear diurnal profile with a maximum at low tide during the daytime. These results represent the first point measurements of IO in the atmosphere by LIF.

Keywords Free-radicals · Iodine monoxide · Laser induced fluorescence · Marine boundary layer · RHaMBLe

L. K. Whalley (✉) · K. L. Furneaux · T. Gravestock · H. M. Atkinson · C. S. E. Bale · T. Ingham · D. E. Heard
School of Chemistry, University of Leeds, Woodhouse Lane, Leeds LS2 9JT, UK
e-mail: L.K.Whalley@leeds.ac.uk

W. J. Bloss
School of Geography, Earth and Environmental Sciences, University of Birmingham, Edgbaston, Birmingham B15 2TT, UK

1 Introduction

The iodine monoxide (IO) radical plays an important role in the chemistry occurring in coastal regions. IO is formed by the reaction of ozone (O_3) with iodine atoms, which are generated via the photolysis of I_2 (Saiz-Lopez and Plane 2004) and photo-labile iodocarbons (Chameides and Davis 1980). IO has been implicated in catalytic O_3 destruction cycles in the marine boundary layer (MBL) (McFiggans et al. 2000), initiated by reaction of the radical with trace gases such as HO_2 and NO_2 as well as with itself. The reaction of IO with HO_2, generating HOI initially, can significantly alter the OH/HO_2 ratio in coastal regions (Bloss et al. 2005) and, therefore, may influence the oxidising capacity of the marine atmosphere. Furthermore, it has been suggested that the reaction product, HOI, may be involved in the autocatalytic release of halogen species from the aerosol phase (Vogt et al. 1999) enhancing O_3 destruction further. The reaction of IO with NO_2 to generate $IONO_2$, which can be taken up on aerosol surfaces, represents an important NO_2 sink, which may be relevant in the NO_x influenced MBL (Platt and Honninger 2003). IO may also play a role in DMS oxidation (particularly under higher IO regimes) (Gravestock et al. 2005; Nakano et al. 2003) and particle formation (O'Dowd et al. 2002). Quantification of these effects requires measurements of the abundance and distribution of IO in marine environments.

To date, the only technique that has successfully detected ambient levels of IO in the MBL is long-path differential optical absorption spectroscopy (DOAS) (Alicke et al. 1999; Allan et al. 2000; Peters et al. 2005; Saiz-Lopez and Plane 2004; Saiz-Lopez et al. 2006a, b), reporting maximum IO concentrations of 7.7 pptV (Peters et al. 2005). In coastal locations, however, the use of the DOAS technique, with typical absorption path-lengths of several kilometres, which may encompass both the open ocean and shoreline environments, raises the debate over inhomogenieties in the sources of the IO precursors. Intertidal regions, which are rich in macroalgae, have been shown to be a major source of I_2 (McFiggans et al. 2004; Saiz-Lopez and Plane 2004) and short-lived iodocarbons (Carpenter et al. 1999, 2001). Local levels of these IO precursor species and in turn local IO levels in these regions (given the short lifetime of the precursors) may be higher than those detected by DOAS, a point first raised by O'Dowd and Hoffmann (2005). Indeed, point measurements of I_2 at Mace Head in Ireland during the 2002 North Atlantic Marine Boundary Layer Experiment (NAMBLEX) campaign by broadband cavity ring-down spectroscopy (BBCRDS) (Langridge et al. 2006) and denuder sampling followed by inductively coupled plasma mass spectrometry (ICP/MS) (Saiz-Lopez et al. 2006a, b) gave concentrations, on average, an order of magnitude greater than I_2 levels detected using the DOAS technique which had a total path-length of 8.4 km. Modelling of the I_2 emissions indicated that the molecular iodine observed by DOAS was concentrated over the intertidal region of the light path (Saiz-Lopez et al. 2006a, b). In support of these findings, Smith et al. (2006) observed an improved agreement between modelled and measured HO_2 concentrations during the campaign when the concentration of the IO radicals was increased tenfold above that measured by DOAS, implying localised shoreline IO production close to where the HO_2 detection cell was located.

The lack of a point source detection method for IO has hampered the quantitative understanding of the processes occurring in the marine environment. Furthermore, the development of a point source instrument could extend the study of IO to more remote regions of the atmosphere, such as the open ocean, where the operation of a long-path DOAS may become less practical.

Bloss et al. (2003) reported the potential of the Laser Induced Fluorescence (LIF) technique for atmospheric detection of IO; this current work presents the first point-source ambient

measurements of IO by LIF. In a separate paper, the first field measurements of IO by cavity ring down spectroscopy (CRDS) are presented by Wada et al. (in press).

2 Experimental

During August and September 2006 the LIF instrument was deployed in Roscoff, Brittany, on the French Atlantic coast, as part of the Reactive Halogens in the Marine Boundary Layer (RHaMBLe) project. Further details of the campaign, including a description of other instruments involved in the project, can be found in McFiggans (2007).

Heard and Pilling 2003). Briefly, the instrument comprises a laser system, a fluorescence cell located on the roof of the container at a height of 3.5 m above sea level at high tide, a detection and data acquisition system and a calibration system.

2.1 Laser system and optics

A wavelength tuneable, Nd:YAG-pumped Ti:Sapphire laser (Photonics Industries) was used to generate light near 445 nm. A complete description of the laser system, including alternative applications for measurement of other species, can be found in Bloss et al. (2003) and so only a brief description is included here.

The Nd:YAG laser produced up to 10 W of 532 nm radiation at a pulse repetition frequency (PRF) of 5 kHz and was used to pump a Ti:Sapphire cavity, resulting in the generation of up to 1.6 W of broadband near-IR radiation. Wavelengths near 890 nm were selected by changing the incident angle of an intra-cavity diffraction grating. Passing radiation at ~890 nm through a cerium lithium borate crystal produced up to 150 mW of the second harmonic at 445 nm. Two beam steering mirrors (CVI, LWP-45-RS445-TP890-PW-1025-C) were used to direct this radiation out of the laser. Typically the beam was ~3 mm in diameter as it exited the laser, with a full width half maximum (FWHM) pulse length of ~35 ns, and a spectral bandwidth of ~0.065 cm^{-1} at 445 nm.

Upon exiting the laser, the blue light was weakly focussed and a small percentage (~5%) was directed to a wavemeter (Coherent Wavemaster) to determine the wavelength (± 0.001 nm) and then directed onto a photodiode (New Focus, 2032 large area photoreceiver), which was housed in a box shielded from ambient light, allowing the laser power to be monitored continuously. The remaining portion of light (~95%) was delivered to the IO fluorescence cell via a fibre optic system consisting of a fibre launcher (Elliot Gold™, MDE511), focussing lens (CVI, PLCX-12.7-11.9-CFUV-308) and fibre (Ocean Optics, P200-10-UV/VIS). Approximately 70% of the incident light was transmitted through a 7 m fibre.

2.2 Fluorescence cell

A diagram of the IO fluorescence cell is presented in Fig. 1. Light exiting the fibre was collimated (Oz Optics HPUCO-25-308-M-25PQ) and directed into the fluorescence region via a baffled side arm (20 cm in length). The baffles, used to reduce the amount of scattered light reaching the channel photo multiplier (CPM) (Perkin Elmer, C993 P), consisted of a series of matt black plastic rings (aperture 5 mm diameter) separated along the arm by spacers. A planoconvex lens with a focal length of 40 cm was located at the entrance of the side arm and reduced the beam diameter to approximately 2 mm at the cell centre. Typically

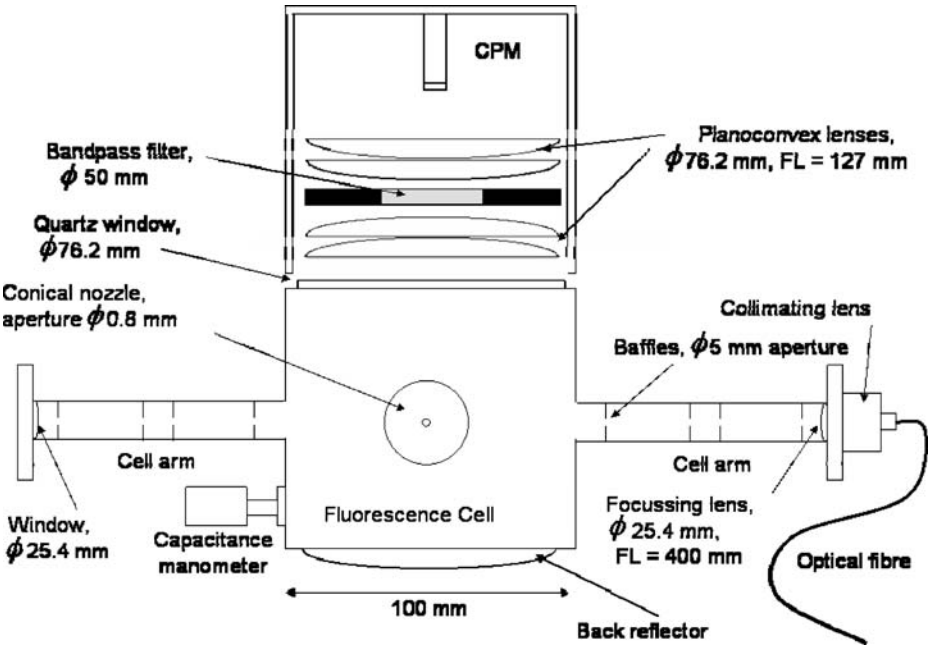

Fig. 1 Plan view of the LIF cell built for the detection of ambient IO. The cell is constructed from a 100× 100×100 mm aluminium cube, anodised matt black. The 4 planoconvex lenses each have a focal length of 127 mm and sandwich the 50 mm diameter 520.3 nm centred bandpass filter. The position of the channel photomultiplier (CPM) with respect to the focussing lenses can be varied to ensure maximum fluorescence collection. The cone-shaped nozzle is raised 10 mm above the fluorescence cell surface and 60 mm above the excitation region. A rotary vane pump is attached to the bottom face of the cell. Laser light exiting the cell is blocked by a beam dump (not shown)

~30 mW of 445 nm radiation reached the cell centre corresponding to 6 μJ per pulse at a 5 kHz PRF.

Sensitivity tests conducted prior to the campaign, which involved throttling the pump to vary the cell pressure, revealed a maximum signal from IO at cell pressures between 120 and 200 Torr. The reduction in sensitivity at the lower pressures was thought to be caused by a reduction in the number density (due to rapid predissociation, quenching is not as significant at lower pressures compared with the detection of molecules like OH), whilst it was speculated that at the higher pressures a change in the expansion geometry may reduce the sensitivity. In view of this, the cell pressure was maintained at around 150 Torr during the campaign to achieve maximum sensitivity.

Ambient air was drawn into the cell at a flow rate of 5 slm (L min^{-1}) via a 0.8 mm aperture at the top of a cone-shaped nozzle of 34.5 mm base diameter and 25.5 mm height. The excitation region of the cell was located 60 mm below the nozzle aperture. During the campaign the nozzle pointed downwards towards the roof of the container, rather than towards the sky, as this was found to reduce the solar radiation detected by the CPM by a factor of 10. The air that reached the nozzle will have been shaded for, at most, 0.5 m or, given a campaign average wind speed of 5 ms^{-1}, 0.1 s. Given an average IO lifetime of 125 s with respect to the IO self reaction, at IO levels of 20 pptV, and an average photolytic lifetime of ~4 s at a solar zenith angle (SZA) of 40° (solar noon) (Laszlo et al. 1995), this shading is felt to have little impact on the IO levels sampled.

The fluorescence detection axis was perpendicular to both the laser beam and ambient airflow and was separated from the cell by a 76.2 mm diameter quartz, broadband (425–675 nm) anti-reflective coated window. Fluorescence from the cell passed along the detection axis, through a 50 mm diameter 520.3 nm centred bandpass filter (FWHM= 10 nm, Melles Griot, 03 FIV 109), and was focussed by a series of four planoconvex lenses (76.2 mm diameter, 127 mm focal length, CVI) onto the photocathode of the yellow sensitised CPM held at −2,900 volts. The signal output from the CPM was sent to a computer controlled photon counter (Stanford Research Systems, SR400), with discriminator level set to −12 mV, to record the signal.

The 520.3 nm bandpass filter effectively discriminated between radiation from the laser pulse and the red-shifted IO fluorescence in the (2,5) band, which directly overlapped in time due to the very short lifetime of the excited state caused by predissociation. The intensity of fluorescence resulting from excitation of a given rotational line in the $A^2\Pi_{3/2} \leftarrow X^2\Pi_{3/2}$ (2,0) band is governed by the groundstate rotational population excited by the laser and the fluorescence quantum yield of the rotational level(s) initially populated. The rate of rotational energy transfer within the $A^2\Pi_{3/2}$ state is small compared with that of predissociation to I + O, but is non-negligible (Gravestock 2006). Although the small rotational constant of the $X^2\Pi_{3/2}$ state of IO, B≈0.34 cm^{-1} (Bekooy et al. 1983; Newman et al. 1998) results in a maximum rotational population of $\boldsymbol{J''}_{max}=17.5$ at room temperature, the (2,0) bandhead is a blend of several rotational transitions ($R_1(2)$, $R_1(3)$, and $R_1(4)$) at the experimental laser linewidth (~0.065 cm^{-1}). As the lifetime of the $A^2\Pi_{3/2}$ state of IO and, hence, the fluorescence quantum yield is inversely proportional to $B\boldsymbol{J'}(\boldsymbol{J'}+1)$ (Bekooy et al. 1983; Newman et al. 1998), excitation of the bandhead yields greatest sensitivity. Further, in the (2,0) band IO does not absorb at frequencies higher than that of the bandhead; thus, tuning the wavelength to a slightly lower wavelength than the bandhead provides an ideal 'offline' background signal.

2.3 Data acquisition

Photons arriving at the CPM were recorded during two time gates. The first gate (100 ns width) was centred directly over the laser pulse (35 ns width) and collected the sum of the LIF signal, laser scattered, and solar scattered light and PMT dark counts. The second gate (1,000 ns width), delayed by 50 μs to a time when the laser pulse and IO fluorescence had subsided, collected the portion solely due to solar scattered light (~0.1 counts s^{-1}) and CPM dark counts (~0 counts s^{-1}), which was then subtracted, after the raw signals had been recorded and saved, from the first gate signal. Tuning the laser wavelength from an 'online' position, which during the campaign was the IO bandhead at 444.887 nm ((Durie and Ramsay 1958), highlighted in Fig. 7), to a region where IO does not absorb ('offline', 444.882 nm) and then subtracting the offline signal from the online provided a signal solely due to LIF from IO.

During the campaign the laser wavelength was tuned to the online wavelength for a period of 150 s, consisting of a sequence of 15, 10 s averaged data points (or 50,000 laser shots), and then tuned offline for another period of 150 s, consisting of a sequence of 15, 10 s averaged data points.

A reference cell was developed to aid the tuning of the laser to the online and offline wavelengths (Bloss et al. 2003). High concentrations of IO were generated by passing a mixture of air, bubbled through CH_3I, through a microwave discharge. Due to difficulties in completely scrubbing the exhaust of the CH_3I, which was being measured by GC-MS downwind of the container, along with other alkyl halides, the reference cell was not operated during the campaign. Instead, tuning the laser between the online and offline

wavelengths was facilitated by means of the wavemeter, which has a precision of ± 0.001 nm. The bandhead of the (2,0) $A^2\Pi_{3/2} \leftarrow X\ ^2\Pi_{3/2}$ transition, centred at 444.887 nm, is a relatively broad structure that spans several wavenumbers as a consequence of being made up of several overlapping rotational lines. Spectral scans of the bandhead revealed that the wavemeter was able to tune repeatedly to at *least* 80% of the line maxima. The imprecision of the wavemeter control of the excitation wavelength introduced an uncertainty of <20% into the measurements. This effect may have contributed to the point-to-point scatter on the data shown below, but will not have biased the average IO levels measured.

In future applications of the instrument a reference cell containing a heated filament which generates IO via CF_3I thermolyisis followed by reaction with O_3 would enable the laser wavelength to be locked at the correct value and would be advantageous for the ambient detection of IO by LIF.

3 Calibration

LIF is not an absolute technique and calibration is therefore required to determine the sensitivity of the instrument. During the campaign calibrations were performed on a daily basis. The signal (S) generated by the instrument is related to [IO] by

$$S = C_{IO} P_w [IO] \tag{1}$$

where C_{IO} is the calibration constant in units of counts s^{-1} mW^{-1} $molecule^{-1}$ cm^3 and P_w is the laser power, in mW, entering the fluorescence cell.

During the calibration a fixed, and known, concentration of IO was generated following photolysis of N_2O (BOC, medical grade), in the presence of CF_3I (Aldrich, 99%), in a 12 slm flow of N_2 (BOC, OFN) at atmospheric pressure. This mixture was flowed through a 25.4 mm internal diameter, 600 mm length quartz flow tube, generating a partially developed laminar flow velocity profile. N_2O was photolysed at 184.9 nm by an Hg pen-lamp (Oriel) housed at the side of the flow tube (Eq. 2). The resulting $O(^1D)$ atoms were quenched rapidly (<1.6 ns) by N_2 to $O(^3P)$ (Eq. 3) and reacted with CF_3I (1 sccm or 82 ppmV), present in excess, to generate IO (Eq. 4). The N_2O was varied from 0.3 to 4 sccm (ml min^{-1}) (or 25–330 ppmV), leading to a range of IO concentrations between 10 and 150 pptV (2.5×10^8–3.8×10^9 molecule cm^{-3}). It is likely that some of the CF_3I will also have been photolysed by the pen-lamp, at 184.9 nm and also by the 253.7 nm Hg line (Hg lines at the longer wavelengths will make a negligible contribution), generating I atoms and CF_3 (Eq. 5). The 254 nm Hg line is 15 times more intense than the 184.9 nm line (Lide 2007), and the CF_3I absorption cross-section is 60 times larger, equal to 4.3×10^{19} cm^2 $molecule^{-1}$ (Rattigan et al. 1997) and, therefore, significant quantities (~4.5×10^{10} molecule cm^{-3}) of CF_3 will be generated at this wavelength. The loss of CF_3I from photolysis will not perturb the IO concentrations generated as CF_3I was kept in excess during the calibration; the loss of IO through reaction with the CF_3 generated (Eq. 6) has been considered (see Section 3.1).

$$N_2O + h\nu_{(184.9\,nm)} \rightarrow N_2 + O(^1D) \tag{2}$$

$$O(^1D) + N_2 \rightarrow O(^3P) + N_2 \tag{3}$$

$$CF_3I + O(^3P) \rightarrow IO + CF_3 \quad (4)$$

$$CF_3I + hv \rightarrow CF_3 + I \quad (5)$$

$$CF_3 + IO \rightarrow LOSS \quad (6)$$

The IO concentration generated at the end of the photolysis region can be calculated using:

$$[IO] = [N_2O]_{cal}\sigma_{N_2O,184.9\,nm}\phi_{IO}F_{184.9\,nm}t \quad (7)$$

where $[N_2O]_{cal}$ is the N_2O concentration used during a calibration point, σ_{N_2O} is the N_2O absorption cross-section, ϕ_{IO} is the chemical yield of IO from the $O+CF_3I$ reaction (=0.83; see Table 1), $F_{184.9\ nm}$ is the photon flux of the lamp at 184.9 nm, and t is the photolysis exposure time.

Rather than the product, $F_{184.9\ nm}\ t$, being measured directly, it was determined using an O_3 actinometer. After the LIF signals for a range of [IO] had been recorded a flow of zero air was added to the calibration gas and the CF_3I flow was switched off. The N_2O was then varied between 0 and 37 sccm (or 0–3,040 ppmV). As the mixture flowed through the photolysis region, O_3 was generated both via

$$O_2 \xrightarrow{184.9\,nm} O + O \quad (8)$$

$$2(O + O_2 + M \rightarrow O_3 + M) \quad (9)$$

for which

$$[O_3]_0 = [O_2]\sigma_{O_2 184.9\,nm}\phi_{O_3}F_{184.9\,nm}t \quad (\phi_{O_3} = 2) \quad (10)$$

Table 1 Reactions and associated rate constants included in the Facsimile model, which was used to assess the formation and potential losses of IO between the photolysis region and sampling nozzle during the calibration

Reaction	Rate constant/cm^3 molecule^{-1} s^{-1}	Reference
$O(^3P)+CF_3I \rightarrow IO+CF_3$	$(0.83 \pm 0.09) \times (7.9 \pm 0.8) \times 10^{-12} \exp[-(175 \pm 40)/T]$	Gilles et al. 1996
$CF_3I+O(^3P) \rightarrow$ other products	$(0.17 \pm 0.09) \times (7.9 \pm 0.8) \times 10^{-12} \exp[-(175 \pm 40)/T]$	Gilles et al. 1996
$IO+IO \rightarrow$ products	$(8.0 \pm 1.5) \times 10^{-11}$	JPL 2006
$IO+O(^3P) \rightarrow I+O_2$	$(1.35 \pm 0.15) \times 10^{-10}$	Canosa-Mas et al. 1999
$CF_3+CF_3(+M) \rightarrow C_2F_6$	$(3.0 \pm 0.4) \times 10^{-12}$	Selamoglu et al. 1986
$CF_3+IO \rightarrow I+CF_3O$	$(0.4 \pm 0.1) \times (1.6 \pm 0.7) \times 10^{-11}$	Vipond et al. 2002
$CF_3+IO \rightarrow$ loss	$(0.6 \pm 0.1) \times (1.6 \pm 0.7) \times 10^{-11}$	Vipond et al. 2002

and, if N_2O was present, via

$$N_2O \xrightarrow{184.9\,nm} N_2 + O(^1D) \tag{11}$$

$$O(^1D) + M \rightarrow O(^3P) + M \tag{12}$$

$$O + O_2 + M \rightarrow O_3 + M \tag{13}$$

leading to the total O_3 generated:

$$[O_3]_{act} = [O_3]_0 + [N_2O]_{act}\sigma_{N_2O,184.9\,nm}\phi_{N_2O}F_{184.9\,nm}t \tag{14}$$

where $\phi_{N_2O} = 1$. If we define $[O_3]_{act}$ as $[O_3]-[O_3]_0$ and $[N_2O]_{act}$ as the N_2O concentration used in the actinometry experiment, then

$$\frac{[O_3]_{act}}{[N_2O]_{act}} = \sigma_{N_2O,184.9\,nm}\phi_{N_2O}F_{184.9\,nm}t \tag{15}$$

and subsequently, by combining equations Eqs. 7 and 15

$$[IO] = \frac{\phi_{IO}}{\phi_{N_2O}}\frac{[O_3]_{act}}{[N_2O]_{act}}[N_2O]_{cal} \tag{16}$$

A commercial O_3 analyser, sampling the excess gas flow, was used to determine the O_3 concentration as the N_2O flow was varied (0–100% on the mass flow controller) during the actinometry experiments, thus providing a relatively simple method of calculating $F_{184.9\ nm}\ t$ and hence [IO]. The addition of N_2O during O_3 actinometry removed the requirement to experimentally determine σ_{O_2}, thus lowering the uncertainty in the calibration. The measurement of σ_{O_2} has previously been shown to be problematic (e.g. Creasey et al. 2000; Lanzendorf et al. 1997). Figure 2 shows a typical plot of $[O_3]$ vs $[N_2O]$. The gradient, $\frac{[O_3]_{act}}{[N_2O]_{act}}$, can be substituted in Eq. 16 to determine [IO].

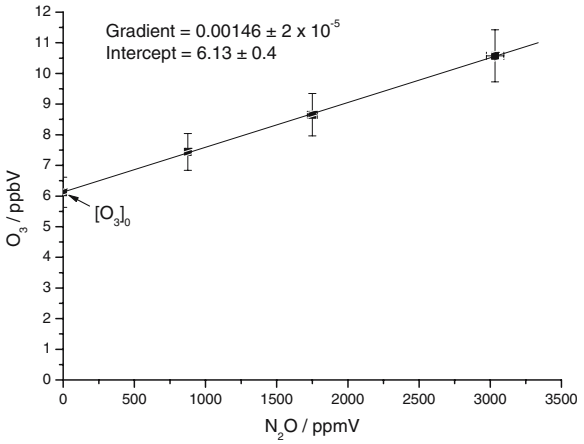

Fig. 2 Typical results from the flow tube actinometry experiment. The gradient, $\frac{[O_3]_{act}}{[N_2O]_{act}}$, can be used to determine the product of the lamp flux (F) and photolysis time (t), Eq. 15, and can be substituted into Eq. 19 to determine the IO concentrations generated during calibrations

3.1 Flow tube losses

Any potential losses of IO between the photolysis region and the nozzle were examined by the use of a numerical model with all relevant IO loss mechanisms included, which are given in Table 1. The simultaneous differential equations were integrated using Facsimile (Curtis and Sweetenham 1987). Over a distance of 4 cm (the distance between the end of the photolysis region and nozzle) at an IO mixing ratio of 150 pptV (or 3.8×10^9 molecule cm^{-3}), the fraction of initially generated IO that was lost was less than 5%, being dominated by the IO self-reaction. Wall losses were investigated by positioning the pen-lamp along the flow-tube at increasing distances from the nozzle and comparing the reduction in IO concentration to model predictions. The best agreement between the experimental data and model was observed when wall loss was not included in the calculations, implying that the loss of the radical to the flow tube walls was minimal. A crucial aspect of this approach was the use of low mixing ratios (<150 pptV), such that the chemical removal of IO was small (<5%) on the timescale of the calibration system flow, and hence any uncertainties arising from the simulation of the IO chemistry, described above, were minimised. The model has also been used to determine the effect CF_3I photolysis (generating CF_3) has upon the IO mixing ratios generated in calibration both at 184.9 nm and 253.7 nm. At 184.9 nm, the absorption cross-section of CF_3I is small, and therefore photolysis of the molecule was found to be unimportant. At 253.7 nm, however, significant quantities of CF_3 molecules were generated (the quantity was dependant on CF_3I concentrations and lamp flux); the reaction of these with IO (Eq. 6) was found to reduce IO mixing ratios by 6±3%. This effect, $LOSS_{CF_3+IO}$, equal to 1.06, has been included in Eq. 16, leading to:

$$[\mathrm{IO}] = \frac{\phi_{\mathrm{IO}}}{\phi_{\mathrm{N_2O}}} \frac{[\mathrm{O_3}]_{\mathrm{act}}}{[\mathrm{N_2O}]_{\mathrm{act}}} \frac{[\mathrm{N_2O}]_{\mathrm{cal}}}{\mathrm{LOSS}_{\mathrm{CF_3+IO}}} \tag{17}$$

3.2 Gas profile factor

For a partially developed laminar flow profile the axial velocity is greatest at the centre of the flow tube and lowest at the edges. These conditions lead to lower IO (and O_3) mixing ratios at the centre of the flow tube than at the edges. This effect may be exacerbated by the potentially non-uniform radial distribution of the lamp flux in the photolysis region. Because the IO fluorescence cell sampled the central portion of the flow (~40% of the total volumetric flow) whilst the O_3 analyser sampled the remaining excess flow, it becomes necessary to know the ratio of

$$P = [\mathrm{O_3}]_{\mathrm{excess}} / [\mathrm{O_3}]_{\mathrm{central}} \tag{18}$$

where P is termed the gas profile factor, and to include this term in Eq. 17 when determining the IO concentrations generated in calibrations:

$$[\mathrm{IO}] = \frac{\phi_{\mathrm{IO}}}{\phi_{\mathrm{N_2O}}} \frac{[\mathrm{O_3}]_{\mathrm{act}}}{[\mathrm{N_2O}]_{\mathrm{act}}} \frac{[\mathrm{N_2O}]_{\mathrm{cal}}}{\mathrm{LOSS}_{\mathrm{CF_3+IO}} P} \tag{19}$$

Holland et al. (2003) found that the P factor varies as a function of flow tube length (which influences the extent to which true laminar flow is established), nozzle aperture and the non-uniform lamp flux across the tube, and, therefore, P needs to be determined experimentally for each individual combination of fluorescence and calibration cells.

It is not possible to measure O_3 that has passed through the IO nozzle under the reduced pressures of the fluorescence cell using a commercial O_3 analyser (Thermo Environmental Instruments TEI 49C) due to the reduction in the O_3 number density and difficulties in achieving suitable flows through the analyser at these pressures. Instead, a commercial NO_x analyser (TEI 42 trace level), inverted to sample O_3, can be employed to sample the O_3 passing through the nozzle and, therefore, determine the *P* factor present in the IO flow tube calibration. Such a method was previously developed by Holland (2005, personal communication). A schematic of the experimental set-up to measure the *P* factor is presented in Fig. 3.

In its normal mode of operation, a NO_x analyser generates an excess flow of ozone in an ozonator and this reacts with NO present in an air sample to generate electronically excited molecules of NO_2 with detection of the resulting fluorescence. Although, typically, the NO detection cell is operated at a pressure of 300 Torr, it is possible to reduce the pressure of the cell further, down to 90 Torr, and still maintain a sufficient flow to the cell to give adequate sensitivity for NO.

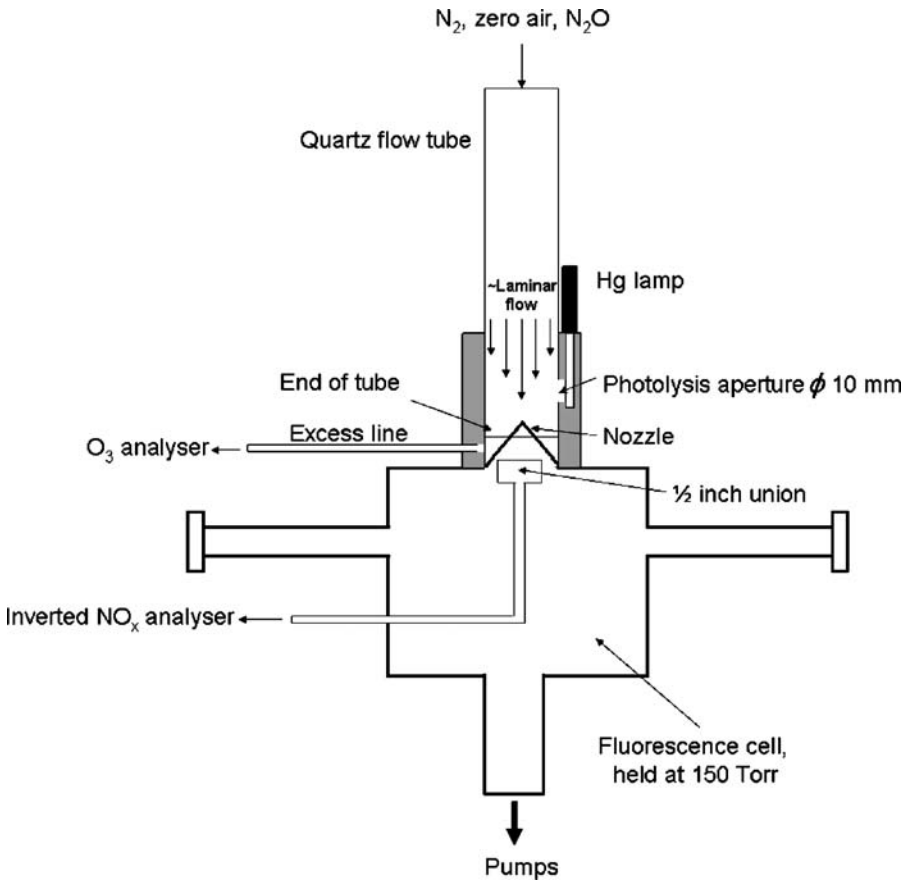

Fig. 3 Schematic of the experimental setup to determine the *P* factor. 12 slm of N_2, zero air and N_2O flowed through the 600 mm quartz tube. N_2O flows were varied between 0 and 37 sccm, generating O_3 mixing ratios in the excess line between 5 and 12 ppbV. The $\phi = 10$ mm photolysis region was 40 mm above the nozzle aperture; the nozzle aperture was 10 mm above the cell and 60 mm above the laser excitation region

Inversion of the NO_x analyser was achieved by replacing the flow of O_3 with a 50 sccm flow of pure NO (Air Products, purity 99.95%) in a 500 sccm flow of N_2 (BOC, OFN). O_3 present in the sample flow reacted with the excess NO supplied, again generating excited state NO_2, the fluorescence from which was detected providing an O_3 measurement. The NO_x analyser was calibrated, at a NO detection cell pressure of ~90 Torr (corresponding to 150 Torr in the LIF cell) and sample flow rate of 150 sccm, against a commercial O_3 analyser running at ambient pressures to determine the sensitivity of the NO_x analyser to O_3 under these conditions. The NO_x analyser was then used to sample the O_3 that had passed through the IO nozzle at 150 Torr, whilst the conventional O_3 analyser was used to determine the O_3 concentration in the excess flow at 760 Torr. By this method the *P* factor was determined to be 2.04±0.11, with the error originating largely from the measurement precision of the O_3 analyser.

3.3 Independent calibration of the instrument

The sensitivity of the IO field instrument has been measured independently with a second calibration system, known as the *wand* system (Edwards et al. 2003; Faloona et al. 2004), in which IO was generated by the same method as outlined in Section 3, but under turbulent flow conditions. In the wand system the Reynolds number=4,259 and velocity=5.4 ms^{-1} whereas in the flow tube system the Reynolds number=704 and velocity=0.4 ms^{-1}. In this manner, the *P* factor determined in the flow tube calibration (Section 3.2), and the simulation of the chemical IO loss (Section 3.1) can be verified. Given the short residence time (~9 ms) under turbulent flows the chemical loss of IO (including loss via Eq. 6) in the wand system was <0.4%.

In the wand calibration system, CF_3I, present in excess (~300 ppmV), was mixed with N_2O (40–383 sccm or 800–7,600 ppmV) in a 50 slm flow of N_2. This gas mixture was passed through a 1.61 cm^2 square internal cross-section flow tube containing an Hg pen-lamp housed behind a Suprasil™ window. The lamp output passed though a series of thin-walled tubes (3 mm internal diameter, 10 mm length), creating an approximately uniform flux throughout the photolysis region. The region surrounding the lamp was flushed with N_2 (g) and heated to 30–40°C to maintain a constant 184.9 nm lamp output. The IO concentration was varied during a calibration both by varying the N_2O concentration in the gas mixture and by varying the lamp current. The product of the flux of the Hg lamp (*F*) and the photolysis time (*t*) was determined by NO actinometry after the calibration.

In the NO actinometry experiment, a turbulent flow of N_2O (5 slm) in N_2 or air (45 slm) was passed through the flow tube, generating NO via:

$$N_2O + h\nu \rightarrow O(^1D) + N_2 \tag{2}$$

$$O(^1D) + N_2O \rightarrow 2NO \tag{20}$$

The $O(^1D)$ atoms are also quenched by collisions with N_2 and O_2; quenching of $O(^1D)$ to $O(^3P)$ by N_2O is not important:

$$O(^1D) + N_2 \rightarrow O(^3P) + N_2 \tag{3}$$

$$O(^1D) + O_2 \rightarrow O(^3P) + O_2 \tag{21}$$

Another loss of $O(^1D)$ is by reaction with N_2O to generate N_2 and O_2 rather than NO

$$O(^1D) + N_2O \rightarrow N_2 + O_2 \tag{22}$$

A small amount of O_2 photolysis will also have occurred in the presence of air, generating O_3 in the system. The flux determined, however, was the same in both air and N_2, demonstrating that this O_3 had minimal effect on the [NO] measured and, hence, the flux calculated.

The product Ft for the wand system was determined using Eq. 23 with an estimated overall uncertainty of ±13% (1σ):

$$Ft = \frac{[NO](k_{R8}[N_2] + k_{R9}[O_2] + (k_{R10} + k_{R7}[N_2O]))}{2k_{R7}\sigma_{N_2O}\phi_{N_2O}[N_2O]^2} \tag{23}$$

In a cross-calibration experiment, the LIF instrument was calibrated initially using the flow tube system to determine its sensitivity, as described in Section 3. The wand system was then used to supply a range of IO mixing ratios, from 17.5 pptV to 160 pptV (or 4.4×10^8–4.0×10^9 molecule cm^{-3}), for sampling by the instrument. The [IO] measured by the field instrument as a function of [IO] supplied by the wand system is shown in Fig. 4, and reveals good agreement, $[IO]_{measured} = 0.87[IO]_{supplied} + 1.63 \times 10^8$ molecule cm^{-3}, between the two calibration methods. The intercept, although not equal to zero, is very small and arises from the random scatter associated with the online and offline signals. The agreement is well within the combined uncertainties of the flow tube calibration (23%, (1σ)) and the uncertainty in [IO] produced by the wand (13%, (1σ)). Table 2 provides a breakdown of the flow tube calibration uncertainties.

The agreement between the two independent calibration methods supports the P factor value determined in Section 3.2 and demonstrates that $\frac{[IO]_{EXCESS}}{[IO]_{CENTRAL}}$ is equivalent to $\frac{[O_3]_{EXCESS}}{[O_3]_{CENTRAL}}$ and, hence, the method used to determine the P factor is valid.

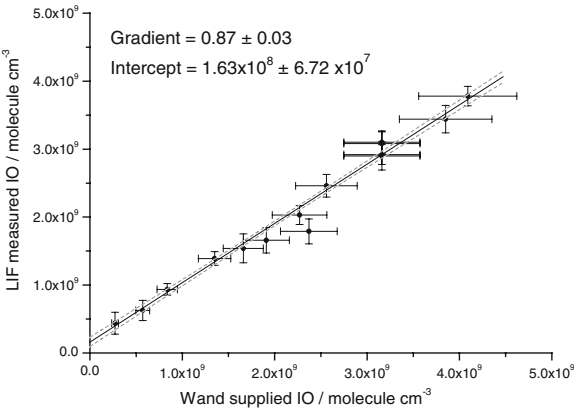

Fig. 4 Results of the cross-calibration experiment. The IO concentrations measured by the LIF instrument, previously calibrated using the flow tube system, are plotted against the supplied IO concentrations from the wand system. The *y-axis error bars* represent the standard deviation of the signal (online–offline) for each concentration supplied, combined with the 1σ flow tube calibration uncertainty (±23% see Table 2). The *x-axis error bars* represent the 13% 1σ wand calibration uncertainty combined with the standard deviation of the concentration supplied. The intercept is non-zero and arises from the random scatter (+/−) associated with the online and offline signals

Table 2 Breakdown of the flow tube calibration uncertainties

Parameter	$\pm 1\sigma$ uncertainty (%)
P_w	1
S	20
ϕ_{IO}	9
ϕ_{N_2O}	<1
$\frac{[O_3]_{act}}{[N_2O]_{act}}$	1.5
$[N_2O]$	2
$LOSS_{CF_3+IO}$	3
P factor	5
C_{IO}/cts s^{-1} molecule^{-1} cm^3 mW^{-1}	23

All uncertainties in the parameters included in Eqs. 1 and 19, which are used to calculate C_{IO} are assessed. The 20% uncertainty assigned to 'S' relates to the variability in the absorption cross-section of the IO bandhead at the laser spectral bandwidth for the wavelength precision (±0.001 nm) achievable by the wavemeter used to control the laser wavelength.

4 Collisional quenching

The first electronically excited state of IO, $A^2\Pi_{3/2}$, is highly predissociative and, therefore, collisional quenching is thought to have a minor impact on the lifetime of the fluorescence. The rate of predissociation, $k_p = 8.5 \times 10^9\ s^{-1}$ at 296 K, whilst the rate of quenching, k_q, is only $3.06 \times 10^9\ s^{-1}$ even in 150 Torr N_2 (Gravestock 2006). In view of this, the instrument sensitivity was expected to be very similar in the presence of N_2 (as in the calibration) and in air (as in ambient sampling mode). Calibrations carried out in a flow of zero air to generate IO, rather than in N_2, suffer from additional chemical complexity due to the generation of O_3, which increases the uncertainty of the calibration. To determine the instrument sensitivity in the presence of N_2 and O_2, therefore, it was necessary to introduce these gases to the bulk flow downstream of the photolysis region. This was facilitated by means of a second flow tube with a side arm below the photolysis region. The ratio of the IO signal (with N_2 added): IO signal (with zero air added) was found to be equal to 0.97±0.16 for a range of sidearm flows (1–10 slm) introduced to the 11 slm bulk flow, indicating that, as expected, the sensitivity of the instrument does not change significantly between N_2 and air.

The impact of H_2O vapour as a potential quencher of IO fluorescence was also investigated. Humidified air was generated by passing zero air through a water bubbler and then mixing this air with a flow of dry zero air to generate a flow with a range of humidities, which was added to the calibration flow, via the sidearm. Over a $[H_2O]$ range of 0% v/v to 1.24% v/v, monitored by a dewpoint hygrometer (General Eastern, Optica), the sensitivity of the LIF instrument remained constant, showing no systematic dependence on H_2O vapour.

The instrument sensitivity for the field data presented in this paper, which is only a subset of the whole set determined during RHaMBLe, was typically $C_{IO} = 2.5 \times 10^{-9}\ cts^{-1} mW^{-1}$ molecule^{-1} cm^3. A typical multi-point calibration taken during the campaign, in which 4 different IO concentrations were generated, is shown in Fig. 5. At a signal-to-noise ratio (SNR) of 1 the average limit of detection (LOD) for a 300 second integration period (total of online and offline period) was typically below 1 pptV, calculated using Eqs. 24 and 25:

$$\mathrm{LOD} = \frac{1}{C_{IO} \times P_w} \sqrt{\left(\frac{1}{m} + \frac{1}{n}\right)} \sigma_b \tag{24}$$

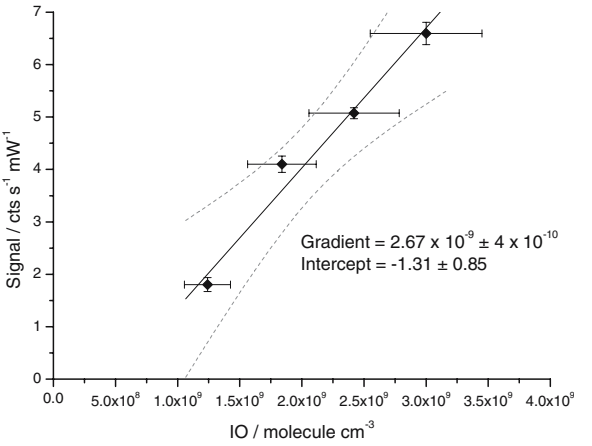

Fig. 5 Typical multi-point calibration showing LIF signal normalised for laser power versus IO concentration supplied by the flow tube calibration cell. The gradient is equivalent to the instrument sensitivity, C_{IO}. *y-axis error bars* represent the standard deviation of the signal (online–offline); *x-axis error bars* represent the 1σ uncertainty in the flow tube calibration method. The intercept is non-zero and arises from the random scatter (+/−) associated with the online and offline signals

where C_{IO} is the instrument sensitivity in counts s^{-1} mW^{-1} $molcule^{-1}$ cm^3, P_w is the laser power entering the cell in mW (P_w=~30 mW), m is the number of data acquisition points taken when the laser is tuned to the online wavelength (m=15), n is the number of data points taken when measuring the background signal (n=15), and σ_b is the sample standard deviation of the background signal:

$$\sigma_b = \sqrt{\frac{1}{t}(S_{lb} + S_{sb} + S_{ds})} \tag{25}$$

where t is the time period for the acquisition of a single data point in seconds (t=10 s), S_{lb} is the laser scatter signal (~50 cts s^{-1}), S_{sb} is the background signal arising from solar scattered light (~0.1 cts s^{-1} at noon), and S_{dc} is the dark count signal of the CPM (~0 cts s^{-1}).

This LOD is comparable (although averaged over a much shorter time period) to that of DOAS (LOD=1 pptV for a 30 min averaging period) reported during the NAMBLEX campaign (Saiz-Lopez et al. 2006a, b).

5 Potential interferences and artefacts

5.1 NO_2 interference

In the blue region of the spectrum where IO absorbs, NO_2 also exhibits a pressure broadened (at 150 Torr) absorption and is known to fluoresce over a wide range of wavelengths, extending to the near IR. A LIF instrument, such as the one described here, could prove an extremely sensitive technique for the detection of ambient NO_2 (Fong and Brune 1997; George and Obrien 1991; Matsumi et al. 2001; Matsumoto et al. 2001; Thornton et al. 2000), particularly when Fluorescence Assay by Gas Expansion (FAGE) is used to expand the sample to low pressures, leading to an extension of the fluorescence lifetime. Ambient NO_2 could potentially interfere with the IO signal observed in this current work if an NO_2 fluorescence signal were to change significantly between the online and offline IO wavelengths. The offline IO wavelength of 444.882 nm, however, was chosen, in part, because

the NO_2 absorption cross-section is extremely similar to that at the online IO wavelength [σ_{NO_2} at 444.882 nm = 6.313×10^{-19} cm^2 molecule^{-1} and σ_{NO_2} at 444.887 nm = 6.315×10^{-19} cm^2 molecule^{-1} at 299 K and 150 Torr (Nizkorodov et al. 2004)]. Furthermore, experiments conducted in which ~3.6 ppmV of NO_2 was added via the calibration cell revealed an increase of around 20 background counts s^{-1} in the spectra between 444.882 nm and 444.887 nm, but with very little additional structure. On average, there was only an increase of 0.001 cts mW^{-1} ppbV^{-1} of NO_2 present (online signal–offline signal), which corresponds to a 0.018 pptV IO artefact per ppbV of NO_2 (assuming an instrument sensitivity of 2.5×10^{-9} cts^{-1}mW^{-1}molecule^{-1}cm^3), well within the uncertainty of the IO measurements given a typical [NO_2] of 0.5 ppbV at the site. The laser was tuned between the online and offline wavelengths every 150 s, and, given the small increase in background counts in the presence of NO_2, an artefact signal may have arisen if ambient NO_2 levels changed significantly in this period. On average, however, there was only a background signal change of ±0.006 cts mW^{-1} ppbV^{-1} of NO_2. This translates to a potential IO artefact of ±0.1 pptV per ppbV change in NO_2. It should be noted that this would only be relevant if NO_2 levels were varying significantly between subsequent online and offline measurements, which in general they were not.

5.2 Laser generated IO

Laser generated IO may form through the laser generation of I atoms, followed by the reaction with ambient O_3, or through direct photolytic production of IO from a suitable precursor. Assuming a bulk gas flow velocity inside the fluorescence cell of 16 cm s^{-1} and a laser beam diameter of 2 mm, an air parcel will take ~1.3×10^{-2} s to pass through the excitation region. The velocity=16 cm s^{-1} was estimated purely from the measured bulk gas flow through the nozzle of 83.3 cm^3 s^{-1} and an estimation of cross-sectional area of the gas beam inside the cell=5.3 cm^2 (Creasey et al. 1997). This velocity takes no account of the rapid acceleration during gas expansion and is, therefore, a lower limit of the much higher velocity experienced. At a PRF of 5 kHz, using a velocity of 16 cms^{-1} a molecule will be hit on average by <63 consecutive laser pulses and, therefore, a source of laser generated I atoms or IO radicals (from suitable precursors) could contribute to the overall IO signal detected. The lifetime of I atoms with respect to reaction with O_3 to form IO is long relative to the time spent in the excitation region (lifetime 4.2 s for 40 ppbv O_3 at the reduced pressure of the fluorescence cell, compared with residence time of 10^{-3} s). Other possible fates for the I atom (e.g. reaction with NO_x) do not lead to immediate IO production and can therefore be neglected. In terms of direct photolytic production of IO, most inorganic iodine species, such as HOI and OIO, do not form IO upon photolysis (Bauer et al. 1998 and Cox et al. 1999 respectively) or do not have significant absorption cross-sections at 445 nm (Bloss et al. 2001), while for other molecules, such as I_2O_2, concentrations in the MBL are expected to be too low to be of significance (Bloss et al. 2003). INO_2 and $IONO_2$ levels may be significant in the MBL, if active iodine chemistry is occurring within an elevated NO_x regime (McFiggans et al. 2000). Under typical conditions during the Roscoff IO measurements, (30 pptV IO and 10 ppbV NO_2), $IONO_2$ concentrations of up to a few ppbV are calculated, depending upon the absorption cross-sections and thermal decomposition rate adopted (Plane 2007, personal communication); however, even at 5 ppb, assuming 100% quantum yield for IO production upon photolysis, an upper limit for the contribution to the measured fluorescence signal from $IONO_2$ is only 0.7% of that from IO; the corresponding figure for INO_2 is 0.4%.

6 Field measurements of IO

During the 2006 RHaMBLe project, the instrument was operated from the 30th August–28th September inclusive. IO was detected at levels above the 300 s LOD of the LIF instrument for significant periods on 11 days when the air sampled had passed over the coast at low tide when the macroalgae in the intertidal region was exposed. A selection of the IO data is presented in this paper to illustrate the performance of the instrument. The dataset will be presented in full, along with a more complete interpretation of the results, in future publications.

Figure 6 shows a series of online/offline spectral modulations during a typical data acquisition, recorded at 10 s resolution on the 7th September at around midday. The contribution due to solar scatter has been subtracted and the data shown have been normalised for laser power fluctuations. A clear modulation between the online and offline wavelengths due to IO fluorescence is observable and corresponds to ~20 pptV of IO. The signal variation observed during the offline acquisition periods represents the random error associated with the instrument precision. The additional variability observed during the online acquisition periods is caused by the ambient IO level variability on short time-scales. An ambient laser excitation spectrum in the wavelength region 444.882–444.894 nm taken on the 14th September (at an IO mixing ratio ~15 pptV) is given in Fig. 7 and shows the IO (2,0) bandhead and other rotational lines overlaid with a laser excitation spectrum recorded during a calibration (IO mixing ratio ~130 pptV). The similarities between the ambient and calibration scans provide further evidence that the LIF signal originates solely from ambient IO. At the time of the scan ambient NO_2 mixing ratios were ~0.54 ppbV and will have contributed no more than 0.01 pptV to the overall IO mixing ratio.

A time series of IO mixing ratios recorded with a 10 s integration period, and plotted with tidal height (calculated hourly), is presented in Fig. 8. An anti-correlation with tidal height is clear, with IO mixing ratios peaking at 27.6±3.2 pptV for one 10 s measurement, just after the lowest tide (the error quoted represents the 1σ calibration uncertainty (23%) combined with the instrument precision (~5%)). Over a 1 hour period, spanning low tide, an average IO mixing ratio of ~12 pptV was recorded. These levels of IO are the highest published to date, indicating, possibly, a localised source of IO precursors. The principal fates of IO in the marine atmosphere are reaction with NO_2, HO_2 and the self-reaction

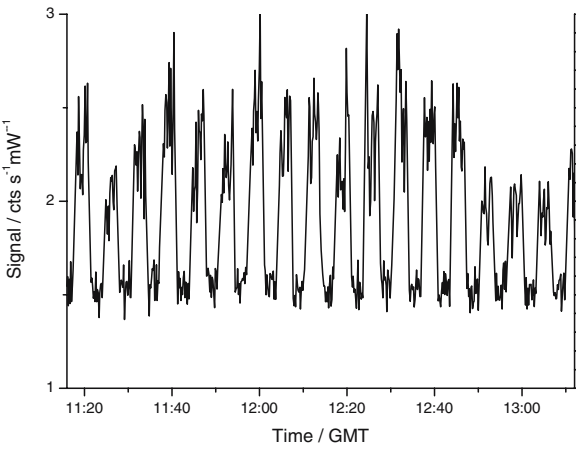

Fig. 6 10 s averaged signal normalised for laser power, with solar scatter subtracted, taken on 7th September 2006, at a laser power of ~55 mW. The plot highlights the clear modulation in signal observed when the wavelength is tuned between the online (15–25 cts $s^{-1}mW^{-1}$) and offline (~12 cts $s^{-1}mW^{-1}$) positions

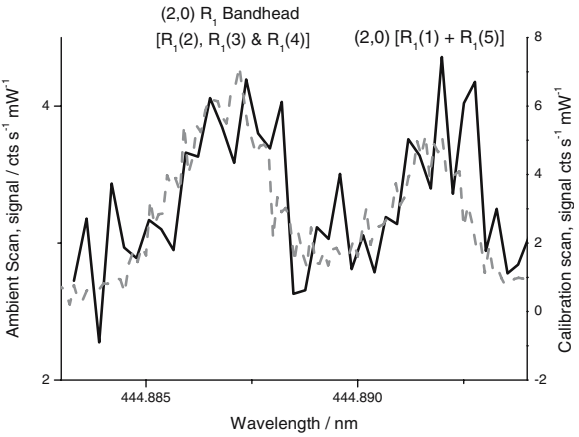

Fig. 7 Laser excitation spectrum of ambient air (*solid line*) between 444.882 and 444.894 nm taken on the 14th September 2006 for an IO concentration ~15 pptV. A spectrum taken during a calibration (*dashed line*) is overlaid for an IO concentration ~130 pptV. The $A^2\Pi_{3/2} \leftarrow X^2\Pi_{3/2}$ (2.0) IO bandhead (*a blend of 3 lines*) and $R_1(1)+R_1(5)$ rotational lines are assigned. The ambient scan took 30 min to complete with each point taken being averaged over 10 s. The overall intensity of the lines in the ambient scan is not totally representative of the IO laser excitation spectrum due to some fluctuations in ambient IO levels during this time

(Eqs. 26, 27, 28, 29, 30, 31, 32 and 33, below), whereas photolysis represents an overall null cycle (Eqs. 34, 35). At levels above a few pptV the IO self-reaction dominates. Under the RHaMBLe conditions the half-life of IO with regard to the self-reaction was 125 s at an IO mixing ratio of 20 pptV. The observed levels of IO (up to 20 pptV, integrated over a 300 s) indicate that either (a) strong IO sources were present in the immediate vicinity of the LIF inlet (for example, molecular iodine or the short-lived iodocarbons, such as CH_2I_2, present at levels of several pptV), or (b) IO levels were sustained for some time in the MBL, following initial formation at a more distant iodine source region, possibly by fast gas-phase reactions such as Eq. 36, as proposed by Plane et al. (2006).

$$IO + HO_2 \rightarrow HOI + O_2 \tag{26}$$

$$HOI + hv \rightarrow I + OH \tag{27}$$

$$I + O_3 \rightarrow IO + O_2 \tag{28}$$

$$IO + NO_2 + M \rightarrow IONO_2 + M \tag{29}$$

$$IONO_2 + hv \rightarrow I + NO_3 \tag{30}$$

$$I + O_3 \rightarrow IO + O_2 \tag{31}$$

$$IO + IO \rightarrow OIO + I \tag{32}$$

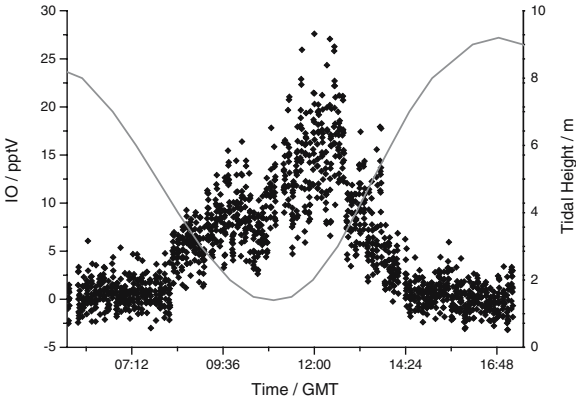

Fig. 8 Time series showing 10 s IO data in pptV (*black diamonds*) taken on the 7th September 2006. Tidal height in meters (*grey solid line*) is overlaid. The 10 s averaged LOD was 1 pptV, at a signal to noise of 1, throughout this day

$$I + O_3 \rightarrow IO + O_2 \tag{33}$$

$$IO + hv \rightarrow I + O \tag{34}$$

$$I + O_3 \rightarrow IO + O_2 \tag{35}$$

$$OIO + NO \rightarrow IO + NO_2 \tag{36}$$

Figure 9 shows three consecutive days and two nights of IO data with the tidal height overlaid. The daytime data are integrated over 300 s (LOD ~ 0.8 pptV on these days) whilst the nighttime data are integrated over 900 s (LOD ~ 0.2 pptV). Again, during the daytime a clear diurnal profile is evident in the IO data, with concentrations peaking at low tide.

During the night IO concentrations were observed to be much lower and rarely exceeded the LOD of the instrument for significant periods even at low tide. On the nights of the 8th and 9th Sept, however, up to 1.8±3.9 pptV of IO was observed just after the low tide for up

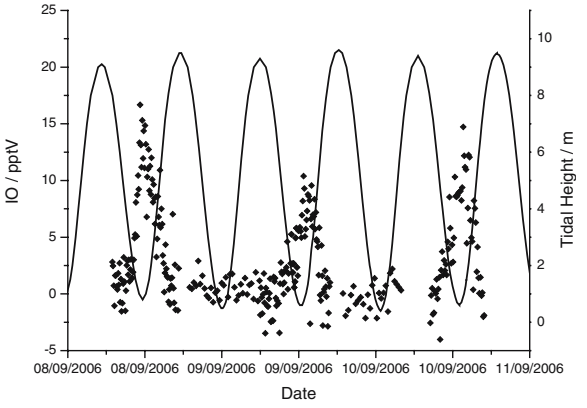

Fig. 9 Time series of IO mixing ratio in pptV (*black diamonds*) showing data from 3 consecutive days and 2 nights from the 8th September to 10th September 2006, inclusive. The error associated with each 300 s point (daytime data) is ~±5.2 and ~±4.6 pptV for each 900 s point (nighttime data) and represents the total calibration uncertainty (23%, 1σ) combined with instrument precision and IO variability during these acquisition periods. The tidal height in meters is overlaid (*solid black line*)

to 1 hr (the error quoted represents the 1σ calibration uncertainty, instrument precision and IO variability during the 900 s data acquisition period). Night-time IO has previously been detected using the DOAS technique at Mace Head on the west coast of Ireland (Saiz-Lopez and Plane 2004) and was attributed to the reaction between I_2 and the NO_3 radical (Chambers et al. 1992), which is assumed to yield INO_3 and I (Atkinson and Wayne 2000). The iodine atom generated can then react with O_3 to form IO. Further interpretation of the night-time data will be the subject of future publications.

7 Summary

A LIF instrument for the in situ measurement of IO radicals with a sub pptV LOD over a 300 s integration period has been described. IO levels at the Roscoff site during RHaMBLe were observed to be typically around 20 pptV during the daytime at low tide if the air sampled had previously passed over the coastline. The results presented here are the first point source, in situ measurements of ambient IO using the LIF technique. The method is extremely sensitive and selective, and therefore ideal for the detection of ambient IO in coastal areas, with potential applications in the open ocean, where IO concentrations are expected to be lower than those reported in this work.

The IO concentrations reported in this work are the highest observed in a coastal environment. Further interpretation of the data through detailed modelling and a comparison with IO concentrations taken during the campaign using LP-DOAS, CRDS and MAX-DOAS will be the subject of future publications. The comparison should provide an insight into the processes occurring in this NO_x influenced coastal environment and should identify possible mechanisms leading to IO production at the shoreline.

Acknowledgements The authors would like to thank Mr P. Halford-Maw and the staff of the workshops within the School of Chemistry for their technical assistance during the development of the IO LIF instrument. Thanks also to Dr. G. McFiggans and Dr. P. Potin, whose campaign and logistical organisation ensured that the RHaMBLe, Roscoff project was a success. The authors wish to acknowledge Roisin Commane and Shona Smith for help in the development of the NO actinometry method. Thanks are also given to Dr. J. Lee for providing the NO_x data prior to publication. KLF acknowledges a NERC studentship. This work was supported by NERC under grant number NE/D006589/1.

References

Alicke, B., Hebestreit, K., Stutz, J., Platt, U.: Iodine oxide in the marine boundary layer. Nature **397**, 572–573 (1999)

Allan, B.J., McFiggans, G., Plane, J.M.C., Coe, H.: Observations of iodine monoxide in the remote marine boundary layer. J. Geophys. Res. **105**, 14363–14369 (2000)

Atkinson, R., Wayne, R. P.: Summary of evaluated kinetic and photochemical data for atmospheric chemistry (2000)

Bauer, D., Ingham, T., Carl, S.A., Moortgat, G.K., Crowley, J.N.: Ultraviolet–visible absorption cross sections of gaseous HOI and its photolysis at 355 nm. J. Phys. Chem. A **102**, 2857–2864 (1998)

Bekooy, J.P., Meerts, W.L., Dymanus, A.: High-resolution laser-Rf spectroscopy on the $A^2\Pi_{3/2}X_2\Pi_{3/2}$ system of iodine oxide (IO). J. Mol. Spectrosc. **102**, 320–343 (1983)

Bloss, W.J., Rowley, D.M., Cox, R.A., Jones, R.L.: Kinetics and products of the IO self-reaction. J. Phys. Chem. A **105**, 7840–7854 (2001)

Bloss, W.J., Gravestock, T.J., Heard, D.E., Ingham, T., Johnson, G.P., Lee, J.D.: Application of a compact all solid-state laser system to the in situ detection of atmospheric OH, HO_2, NO and IO by laser-induced fluorescence. J. Environ. Monit. **5**, 21–28 (2003)

Bloss, W.J., Lee, J.D., Johnson, G.P., Sommariva, R., Heard, D.E., Saiz-Lopez, A., Plane, J.M.C., McFiggans, G., Coe, H., Flynn, M., Williams, P., Rickard, A.R., Fleming, Z.L.: Impact of halogen monoxide chemistry upon boundary layer OH and HO_2 concentrations at a coastal site. Geophys. Res. Lett. **32**, L06814 (2005) doi: 10.1029/2004GL022084

Canosa-Mas, C.E., Flugge, M.L., Shah, D., Vipond, A., Wayne, R.P.: Kinetics of the reactions of IO with HO_2 and $O(^3P)$. J. Atmos. Chem. **34**, 153–162 (1999)

Carpenter, L.J., Sturges, W.T., Penkett, S.A., Liss, P.S., Alicke, B., Hebestreit, K., Platt, U.: Short-lived alkyl iodides and bromides at Mace Head, Ireland: links to biogenic sources and halogen oxide production. J. Geophys. Res. **104**, 1679–1689 (1999)

Carpenter, L.J., Hebestreit, K., Platt, U., Liss, P.S.: Coastal zone production of IO precursors: a 2-dimensional study. Atmos. Chem. Phys. **1**, 9–18 (2001)

Chambers, R.M., Heard, A.C., Wayne, R.P.: Inorganic gas-phase reactions of the nitrate radical: I_2+NO_3 and $I+NO_3$. J. Phys. Chem. **96**, 3321–3331 (1992)

Chameides, W.L., Davis, D.D.: Iodine – its possible role in tropospheric photochemistry. J. Geophys. Res. **85**, 7383–7398 (1980)

Cox, R.A., Bloss, W.J., Jones, R.L., Rowley, D.M.: OIO and the atmospheric cycle of iodine. Geophys. Res. Lett. **26**, 1857–1860 (1999)

Creasey, D.J., Heard, D.E., Pilling, M.J., Whitaker, B.J., Berzins, M., Fairlie, R.: Visualisation of a supersonic free-jet expansion using laser-induced fluorescence spectroscopy: application to the measurement of rate constants at ultralow temperatures. Appl. Phys. B **65**, 375–391 (1997)

Creasey, D.J., Heard, D.E., Lee, J.D.: Absorption cross-section measurements of water vapour and oxygen at 185 nm. Implications for the calibration of field instruments to measure OH, HO_2 and RO_2 radicals. Geophys. Res. Lett. **27**, 1651–1654 (2000)

Curtis, A.R., Sweetenham, W.P.: H. M. Stationary Office (1987)

Durie, R.A., Ramsay, D.A.: Absorption spectra of the halogen monoxides. Can. J. Phys. **36**, 35 (1958)

Edwards, G.D., Cantrell, C.A., Stephens, S., Hill, B., Goyea, O., Shetter, R.E., Mauldin, R.L., Kosciuch, E., Tanner, D.J., Eisele, F.L.: Chemical ionization mass spectrometer instrument for the measurement of tropospheric HO_2 and RO_2. Anal. Chem. **75**, 5317–5327 (2003)

Faloona, I.C., Tan, D., Lesher, R.L., Hazen, N.L., Frame, C.L., Simpas, J.B., Harder, H., Martinez, M., Di Carlo, P., Ren, X.R., Brune, W.H.: A laser-induced fluorescence instrument for detecting tropospheric OH and HO_2: characteristics and calibration. J. Atmos. Chem. **47**, 139–167 (2004)

Fong, C., Brune, W.H.: A laser induced fluorescence instrument for measuring tropospheric NO_2. Rev. Sci. Instrum. **68**, 4253–4262 (1997)

George, L.A., Obrien, R.J.: Prototype FAGE determination of NO_2. J. Atmos. Chem. **12**, 195–209 (1991)

Gilles, M.K., Turnipseed, A.A., Talukdar, R.K., Rudich, Y., Villalta, P.W., Huey, L.G., Burkholder, J.B., Ravishankara, A.R.: Reactions of $O(^3P)$ with alkyl iodides: rate coefficients and reaction products. J. Phys. Chem. **100**, 14005–14015 (1996)

Gravestock, T.: A kinetic and spectroscopic study of chemistry relating to the atmospheric role of iodine species. PhD Thesis University of Leeds (2006)

Gravestock, T., Blitz, M.A., Heard, D.E.: Kinetics study of the reaction of iodine monoxide radicals with dimethyl sulfide. Phys. Chem. Chem. Phys. **7**, 2173–2181 (2005)

Heard, D.E., Pilling, M.J.: Measurement of OH and HO_2 in the troposphere. Chem. Rev. **103**, 5163–5198 (2003)

Holland, F., Hofzumahaus, A., Schafer, J., Kraus, A., Patz, H.W.: Measurements of OH and HO_2 radical concentrations and photolysis frequencies during BERLIOZ. J. Geophys. Res. **108**, 8246–8267 (2003)

JPL. Chemical kinetics and photochemical data for use in atmospheric studies evaluation, number 15, 42 (2006)

Langridge, J.M., Ball, S.M., Jones, R.L.: A compact broadband cavity enhanced absorption spectrometer for detection of atmospheric NO_2 using light emitting diodes. Analyst **131**, 916–922 (2006)

Lanzendorf, E.J., Hanisco, T.F., Donahue, N.M., Wennberg, P.O.: The measurement of tropospheric OH radicals by laser-induced fluorescence spectroscopy during the POPCORN field campaign and intercomparison of tropospheric OH radical measurements by multiple folded long-path laser absorption and laser induced fluorescence – comment. Geophys. Res. Lett. **24**, 3037–3038 (1997)

Laszlo, B., Kurylo, M.J., Huie, R.E.: Absorption cross-sections, kinetics of formation, and self-reaction of the IO radical produced via the laser photolysis of $N_2O/I_2/N_2$ mixtures. J. Phys. Chem. **99**, 11701–11707 (1995)

Lide, D.R. (ed.): CRC Handbook of Chemistry and Physics, Internet Version 2007, 87th edn. Taylor and Francis, Boca Raton, FL (2007) http://www.hbcpnetbase.com

Matsumi, Y., Murakami, S., Kono, M., Takahashi, K., Koike, M., Kondo, Y.: High-sensitivity instrument for measuring atmospheric NO_2. Anal. Chem. **73**, 5485–5493 (2001)

Matsumoto, J., Hirokawa, J., Akimoto, H., Kajii, Y.: Direct measurement of NO_2 in the marine atmosphere by laser-induced fluorescence technique. Atmos. Environ. **35**, 2803–2814 (2001)

McFiggans, G., The RHaMBLe Coastal Team: Iodine-mediated ultrafine particle formation in the RHaMBLe Roscoff 2007 coastal experiment. Geophys. Res. Abstr. **9**, 10701 (2007)

McFiggans, G., Plane, J.M.C., Allan, B.J., Carpenter, L.J., Coe, H., O'Dowd, C.: A modeling study of iodine chemistry in the marine boundary layer. J. Geophys. Res. **105**, 14371–14385 (2000)

McFiggans, G., Coe, H., Burgess, R., Allan, J., Cubison, M., Alfarra, M.R., Saunders, R., Saiz-Lopez, A., Plane, J.M.C., Wevill, D.J., Carpenter, L.J., Rickard, A.R., Monks, P.S.: Direct evidence for coastal iodine particles from Laminaria macroalgae – linkage to emissions of molecular iodine. Atmos. Chem. Phys. **4**, 701–713 (2004)

Nakano, Y., Enami, S., Nakamichi, S., Aloisio, S., Hashimoto, S., Kawasaki, M.: Temperature and pressure dependence study of the reaction of IO radicals with dimethyl sulfide by cavity ring-down laser spectroscopy. J. Phys. Chem. A **107**, 6381–6387 (2003)

Newman, S.M., Howie, W.H., Lane, I.C., Upson, M.R., Orr-Ewing, A.J.: Predissociation of the $A^2\Pi_{3/2}$ state of IO studied by cavity ring-down spectroscopy. J. Chem. Soc. Faraday Trans. **94**, 2681–2688 (1998)

Nizkorodov, S.A., Sander, S.P., Brown, L.R.: Temperature and pressure dependence of high-resolution air-broadened absorption cross sections of NO_2 (415–525 nm). J. Phys. Chem. A **108**, 4864–4872 (2004)

O'Dowd, C.D., Hoffmann, T.: Coastal new particle formation: a review of the current state-of-the-art. Environ. Chem. **2**, 245–255 (2005)

O'Dowd, C.D., Jimenez, J.L., Bahreini, R., Flagan, R.C., Seinfeld, J.H., Hameri, K., Pirjola, L., Kulmala, M., Jennings, S.G., Hoffmann, T.: Marine aerosol formation from biogenic iodine emissions. Nature **417**, 632–636 (2002)

Peters, C., Pechtl, S., Stutz, J., Hebestreit, K., Honninger, G., Heumann, K.G., Schwarz, A., Winterlik, J., Platt, U.: Reactive and organic halogen species in three different European coastal environments. Atmos. Chem. Phys. **5**, 3357–3375 (2005)

Plane, J.M.C., Joseph, D.M., Allan, B.J., Ashworth, S.H., Francisco, J.S.: An experimental and theoretical study of the reactions OIO plus NO and OH plus OH. J. Phys. Chem. A **110**, 93–100 (2006)

Platt, U., Honninger, G.: The role of halogen species in the troposphere. Chemosphere **52**, 325–338 (2003)

Rattigan, O.V., Shallcross, D.E., Cox, R.A.: UV absorption cross-sections and atmospheric photolysis rates of CF_3I, CH_3I, C_2H_5I and CH_2ICl. J. Chem. Soc. Faraday Trans. **93**, 2839–2846 (1997)

Saiz-Lopez, A., Plane, J.M.C.: Novel iodine chemistry in the marine boundary layer. Geophys. Res. Lett. **31**, L04112 (2004) doi: 10.1029/2003GL019215

Saiz-Lopez, A., Shillito, J.A., Coe, H., Plane, J.M.C.: Measurements and modelling of I_2, IO, OIO, BrO and NO_3 in the mid-latitude marine boundary layer. Atmos. Chem. Phys. **6**, 1513–1528 (2006a)

Saiz-Lopez, A., Plane, J.M.C., McFiggans, G., Williams, P.I., Ball, S.M., Bitter, M., Jones, R.L., Hongwei, C., Hoffmann, T.: Modelling molecular iodine emissions in a coastal marine environment: the link to new particle formation. Atmos. Chem. Phys. **6**, 883–895 (2006b)

Selamoglu, N., Rossi, M.J., Golden, D.M.: Absolute rate of recombination of CF_3 radicals. Chem. Phys. Lett. **124**, 68–72 (1986)

Smith, S.C., Lee, J.D., Bloss, W.J., Johnson, G.P., Ingham, T., Heard, D.E.: Concentrations of OH and HO_2 radicals during NAMBLEX: measurements and steady state analysis. Atmos. Chem. Phys. **6**, 1435–1453 (2006)

Thornton, J.A., Wooldridge, P.J., Cohen, R.C.: Atmospheric NO_2: in situ laser-induced fluorescence detection at parts per trillion mixing ratios. Anal. Chem. **72**, 528–539 (2000)

Vipond, A., Canosa-Mas, C.E., Flugge, M.L., Gray, D.J., Shallcross, D.E., Shah, D., Wayne, R.P.: A discharge-flow study of the self-reaction of IO. Phys. Chem. Chem. Phys. **4**, 3648–3658 (2002)

Vogt, R., Sander, R., Von Glasow, R., Crutzen, P.J.: Iodine chemistry and its role in halogen activation and ozone loss in the marine boundary layer: a model study. J. Atmos. Chem. **32**, 375–395 (1999)

Wada, R., Beames, J.M., Orr-Ewing, A.J.: Measurement of IO radical concentrations in the marine boundary layer using a cavity ring-down spectrometer. J. Atmos. Chem. (in press)